ChemPubSoc Europe

DOI: 10.1002/cctc.201600762

CHEMCATCHEM Full Papers

Reaction and Mechanistic Studies of Heterogeneous Hydroamination over Support-Stabilized Gold Nanoparticles

Manideepa Sengupta,[a] Arijit Bag,[b] Subhasis Das,[a] Astha Shukla,[a] L. N. Sivakumar Konathala,[a] C. A. Naidu,[a] and Ankur Bordoloi*[a]

Highly stable gold nanoparticles (GNPs) around 5–6 nm have been prepared by in situ reduction of chloroauric acid on the surface of nitrogen-rich mesoporous carbon (MCN) without adding any extra stabilizing agent. The synthesized materials have been efficiently utilized as a catalyst for the truly heterogeneous hydroamination of phenylacetylene with aniline. Large turnover numbers (42×10^6) were achieved by suitably adjusting the gold/support (w/w) ratio, time, temperature, and solvent, leading to 98% selectivity towards the Markovnikov product. Density functional theory (DFT) studies have been performed to predict the mechanistic pathway of hydroamination with Au^0 in GNP@MCN. To understand the structure–activity relationship, the catalyst was characterized by using different techniques such as X-ray diffraction (XRD), scanning electron microscopy (SEM), transmission electron microscopy (TEM), nitrogen physisorption studies (BET), X-ray photoelectron spectroscopy (XPS), and Fourier transform infrared (FTIR) spectroscopy.

1. Introduction

Catalysis with gold nanoparticles (GNPs) is a subject of substantial current interest and use of GNP-based catalysts has been widely explored in recent years.[1] However, gold was traditionally viewed as catalytically inactive for a long time;[2] this changed after Bond et al.,[3] in 1973, reported gold was active for olefin hydrogenation if dispersed as small nanoparticles. More than a decade later, another milestone in heterogeneous catalysis was established when Haruta et al.[4] demonstrated the low-temperature oxidation of carbon monoxide and Hutchings[5] showed the extraordinary catalytic activity of gold for the hydrochlorination of ethyne to vinyl chloride. Since then, interest in gold catalysis has grown exponentially and over the past few years gold has emerged as a source of effective homogeneous[6] and heterogeneous[7] catalysts. Although the bulk metal is largely non-active in catalysis,[8] GNPs, however, exhibit high catalytic activity, high reaction selectivity, and also provide low reaction temperatures, which depend mainly on the particle size and the support used.[2,9]

Hydroamination, the addition of N–H bonds across C–C multiple bonds[10] is of considerable interest in organic chemistry as the reaction enables the synthesis of organo-nitrogen compounds such as enamines, imines, and alkylated amines, which are widely present as chemical intermediates in the field of natural products, pharmacological agents, polymers, dyes, agrochemicals, cosmetics, and fine chemicals.[11] Both the Markovnikov and anti-Markovnikov addition products provide biological and pharmaceutical activity. Even if hydroamination merges thermodynamic feasibility along with 100% atom economy owing to no formation of any byproducts such as water and salts, the reaction still has a considerable kinetic barrier and hence the use of a catalyst is the desired option.

The nucleophilic addition of amines across C–C multiple bonds is kinetically difficult owing to the repulsion between the high electron density of the amine and the π-electrons of the multiple bonds.[12] Although considerable progress has been made by using metals and metal complex catalysts under homogeneous conditions, nevertheless, only a few heterogeneous catalysts[13] are reported in the literature. Recently, Rodionov et al.[14] reported the hydroamination of alkynes with anilines by using $Au@SiO_2$ as a catalyst. Zhu et al.[15] reported photolytic hydroamination over Au/TiO_2, however, the turnover numbers were found to be quite low.

Herein, gold nanoparticles have been incorporated on nitrogen-rich mesoporous carbon (GNP@MCN), which acts as a stabilizing and size-controlling agent and thus gold nanoparticles of particle size 5–6 nm have been synthesized without the addition of an external stabilizing agent. The inner surface of the mesoporous walls of MCN provides nitrogen functionalities, which stabilize GNPs[16] (Scheme 1) and with this synthesized catalyst, GNP@MCN, the hydroamination reaction of phenylacetylene with aniline was performed. Moreover, a computational approach has been used to understand the reaction path-

[a] M. Sengupta, S. Das, A. Shukla, L. N. S. Konathala, C. A. Naidu, Dr. A. Bordoloi
Refinery Technology Division
CSIR-Indian Institute of Petroleum
Dehradun-248005 Uttarakhand (India)
E-mail: ankurb@iip.res.in

[b] Dr. A. Bag
Chemical Science Division
IISER Kolkata
Mohanpur, Nadia, West Bengal (India)

Supporting information for this article can be found under http://dx.doi.org/10.1002/cctc.201600762.

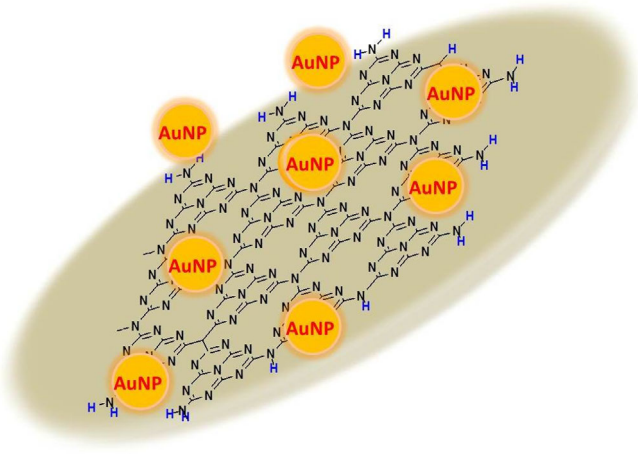

Scheme 1. Incorporation of gold nanoparticles over nitrogen-rich mesoporous carbon (GNP@MCN).

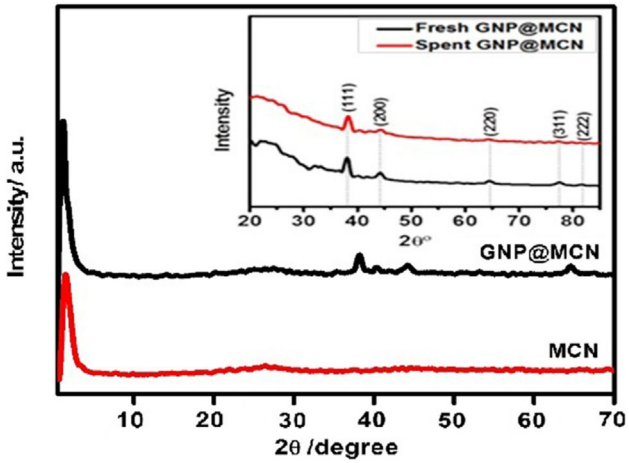

Figure 1. Low- and wide-angle powder XRD patterns of MCN and GNP@MCN.

ways of selective heterogeneous hydroamination over an Au^0 catalyst system for the first time.

The catalyst system (GNP@MCN) exhibits high reactivity and over 98% selectivity towards the Markovnikov addition product, phenyl-(1-phenylethylidine) amine **A** (Scheme 2).

2. Results and Discussion

2.1. Characterization of catalyst

2.1.1. Structure and morphology of GNP@MCN

The low-angle XRD patterns for both MCN and GNP@MCN exhibit a sharp peak within the range 0.5–6° (indexed as the (100) reflection of the hexagonal *p6mm* space group), indicating that the hexagonal ordered porous structure of MCN remains intact even after incorporation of gold nanoparticles. The wide-angle XRD pattern of GNP-loaded MCN displays five peaks, which could be indexed as the (111), (200), (220), (311), and (222) reflections of the face centered cubic structure of crystalline Au^0 (JCPDS Card No. 89-3697; Figure 1, inset). The weak and broad peaks also indicate the formation of small gold nanoparticles within the mesoporous channels of the nitrogen-rich carbon. The absence of any sharp peaks confirms no aggregation of the GNPs and no large particles were formed on the surface of the MCN. In the XRD pattern, the (111) peak is the strongest, indicating that the (111) plane is the predominant crystal facet. Both the low- and wide-angle XRD patterns show a broad peak around 26°, which could be indexed to the (002) plane of graphitic carbon.[17] The peaks recorded from wide-angle powder XRD of both the fresh and spent catalysts were also the same, which implies that there was no alteration of the morphology of the catalyst and hence it was stable and active for hydroamination.

To understand the morphology and structure, scanning electron microscopy (SEM) images of the catalyst GNP@MCN were taken. Energy-dispersive X-ray spectroscopy (EDX) was used in connection with SEM for the elemental analysis. White dots corresponding to gold nanoparticles are distributed uniformly over the mesoporous nitrogen-rich carbon; no agglomeration of the gold nanoparticles was seen, which also confirms that the size of the gold nanoparticles was controlled and stabilized by the –NH and $–NH_2$ units of MCN (Figure 2e–f). SEM images for the template SBA-15 (Figure 2a–b) and support MCN (Figure 2c–d) were also taken, which reveal that the typical rod-like morphology of SBA-15 was well replicated in the support MCN and also in the catalyst GNP@MCN, even after encapsulation of gold nanoparticles within the nanochannels of MCN. Thus, the successful replication and formation of ordered mesostructures were also confirmed by SEM. The presence of peaks only for C, N, and Au and the absence of peaks for Cl and Na in EDX spectroscopy (Figure S1, in the Supporting Information) signify the purity of the catalyst.

The particle size and GNP distribution within the nanochannels of MCN were analyzed by transmission electron microscopy (TEM). High-resolution (HR)-TEM images of GNP@MCN (2 wt% Au loading) are shown in Figure 3b–d, f. The black

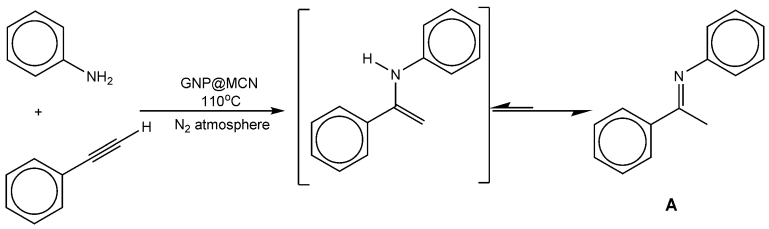

Scheme 2. Supported Au catalysis of phenylacetylene with aniline.

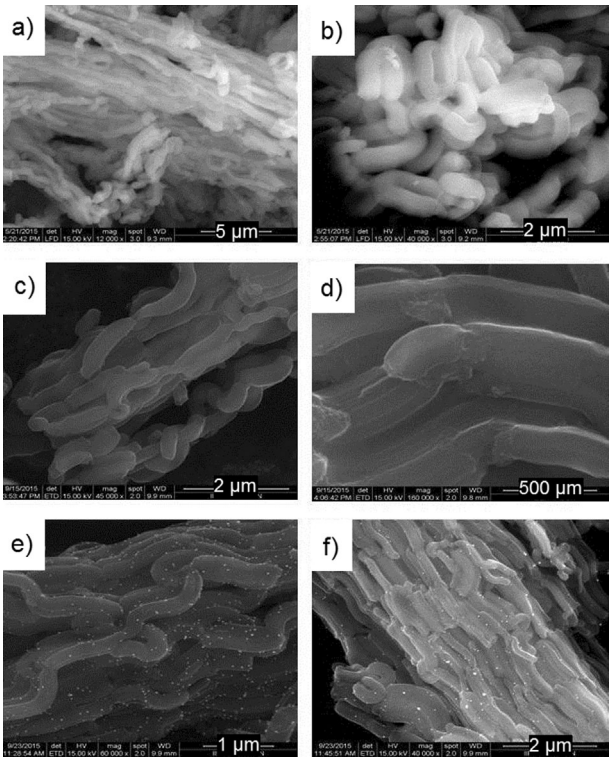

Figure 2. FE-SEM images of (a, b) SBA-15, (c, d) MCN, and (e, f) GNP@MCN.

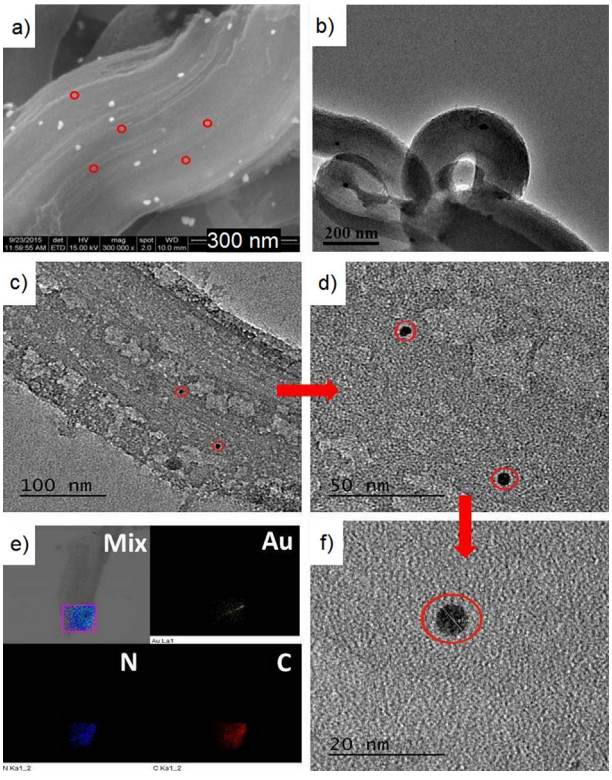

Figure 3. (a) FE-SEM image, (b, c, d, f) TEM images, and (e) elemental mapping of GNP@MCN.

dots corresponding to gold nanoparticles; the average size of the particles obtained from HR-TEM was around 5–6 nm. However, on increasing the amount of gold loading, agglomeration of gold nanoparticles over the surface of the support was found. The field emission (FE)-SEM image of GNP@MCN (4 wt% Au loading, Figure 3a) exhibits particles of 15–25 nm originating from the aggregation of the same over the surface of the support and particles of sizes less than 10 nm are present within the mesochannels of MCN. Elemental mapping shows that the Au nanoparticles are well implanted in the MCN (Figure 3e).

The XPS survey scan of GNP@MCN (Figure 4a) is composed of peaks at 85.08, 88.08, 285.08, 399.08, and 533.08 eV, which correspond to Au $4f_{7/2}$, Au $4f_{5/2}$, C 1s, N 1s, and O 1s, respectively, which confirms the presence of gold, carbon, nitrogen, and some surface oxygen.[18] Higher resolution XPS spectra of C 1s, N 1s, and Au 4f are also shown in Figure 4 and the spectra were deconvoluted. The C 1s spectrum was deconvoluted into four components at binding energies of 284.3, 285.5, 286.7, and 288.3 eV (Figure 4b).

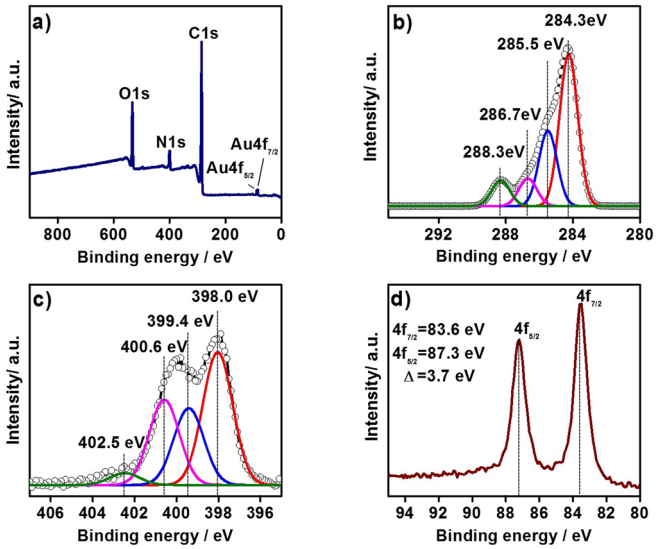

Figure 4. (a) XPS survey scan and XPS curves of (b) C 1s, (c) N 1s, and (d) Au $4f_{5/2}$, Au $4f_{7/2}$ of GNP@MCN.

The two main peaks at 284.3 and 285.5 eV correspond to sp^2-hybridized graphite-like carbon (C–C sp^2) and sp^3-hybridized diamond-like carbon (C–C sp^3), respectively. However, the peaks at 286.7 and 288.3 eV are a result of the presence of oxygen groups (as C–O, C=O, and –COO) on the surface.[19] The N 1s area (Figure 4c) reveals three major peaks at 398.0, 399.4, 400.6 eV, which relate to pyridinic, pyrrolic, and quaternary nitrogen, respectively, whereas the minor peak at 402.5 eV originates from the N-oxide of the pyridinic nitrogen.[19a,b] The Au 4f scan (Figure 4d) exhibits two sharp peaks at 83.6 eV (Au $4f_{7/2}$) and 87.3 eV (Au $4f_{5/2}$), which confirms the presence of gold in the 0 oxidation state in GNP@MCN.[18]

The specific surface area of MCN before and after incorporation of gold nanoparticles was evaluated by measuring nitro-

gen adsorption–desorption isotherms and was found to decrease from 400 $m^2 g^{-1}$ to 360 $m^2 g^{-1}$. At the same time, a decrease in the specific pore volume from 0.39 to 0.36 $cm^3 g^{-1}$ and an increase in specific pore diameter from 3.5 nm to 5.6 nm was found, which could a result of the formation of gold nanoparticles inside the pores of MCN (Table 1). The absence of any drastic change in the specific surface area and pore volume also supports the idea that gold nanoparticles were formed within the pores of the MCN and the pores of the MCN are not blocked by gold particles, which reveals that there was no agglomeration of the gold particles.

Table 1. Specific surface area, specific pore volume, and specific pore diameter for MCN and GNP@MCN.

Entry	Sample	Specific surface area [$m^2 g^{-1}$]	Specific pore volume [$cm^3 g^{-1}$]	Specific pore diameter [nm]
1	MCN	400	0.39	3.5
2	GNP@MCN	360	0.36	5.6

The existence of nitrogen functionalities was also confirmed by performing FTIR spectroscopy. The FTIR spectra (Figure 5) of the GNP@MCN and MCN samples showed similar vibration peaks. Both the samples showed broad peaks around 3000–3500 cm^{-1}, which are assigned to the stretching vibration mode of –NH and $–NH_2$ units. The infrared absorption bands around 1415 cm^{-1} and 1614 cm^{-1} represent the C–N and C=N stretching frequencies, respectively.[20] However, a minor shift in absorption bands in GNP@MCN compared with that of pure MCN was observed, which may arise from the incorporation of gold nanoparticles within the mesochannels of MCN.

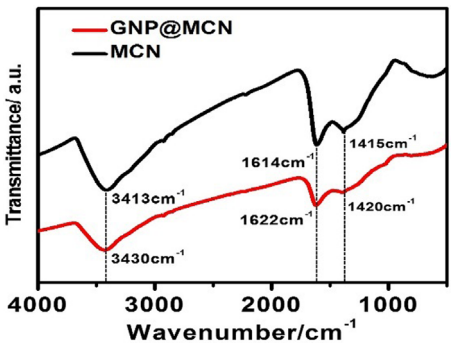

Figure 5. FTIR spectra of MCN and GNP@MCN.

2.2. Hydroamination of phenylacetylene

To explore the potential of the catalyst GNP@MCN, hydroamination of phenylacetylene was carried out under reflux conditions under a nitrogen atmosphere and the reaction conditions were optimized. The effect of catalyst, substrate concentration, amount of solvent, temperature, and pressure on the hydroamination of phenylacetylene with aniline over GNP@MCN was studied:

(i) The temperature was varied between 90 and 130 °C, while keeping the amount of catalyst (2 wt% with respect to (w.r.t.) phenylacetylene, 0.1×10^{-2} mmol of Au) and ratio of phenylacetylene and aniline (1:2) constant (Figure 6a). A linear increase in the rate of phenylacetylene conversion was observed with increasing temperature from 90 to 130 °C over a period of 24 h. After this, a steady state was observed for 130 °C with a maximum conversion of 95% and almost 100% selectivity, whereas a further increase in conversion was observed for other reaction temperatures (90 °C and 110 °C).

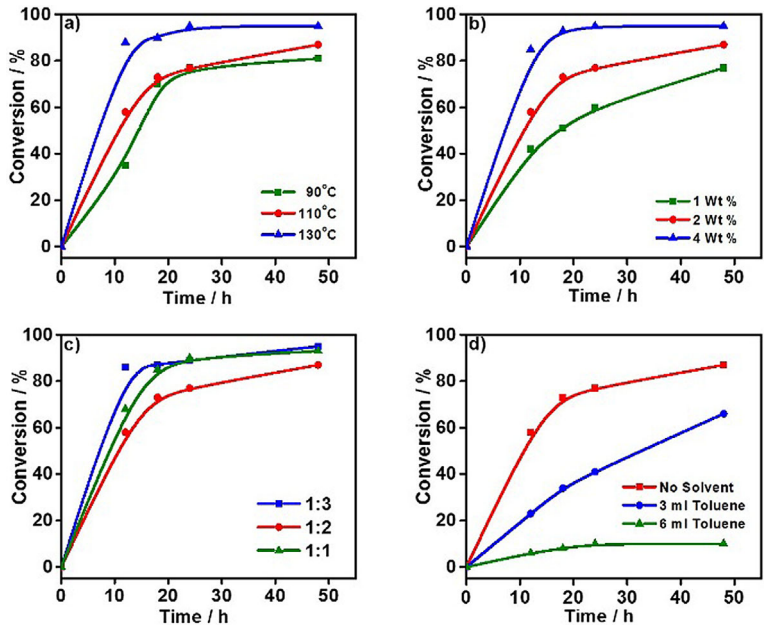

Figure 6. Effect of (a) temperature variation, (b) catalyst concentration variation, (c) molar ratio variation of the reactants, and (d) amount of solvent on the hydroamination reaction of phenylacetylene with aniline by using GNP@MCN as the catalyst.

(ii) While keeping the reaction temperature at 110 °C and the mole ratio of phenylacetylene and aniline (1:2) constant, the catalyst amount was varied from 1 wt% to 4 wt% w.r.t. phenylacetylene. A linear increase in the conversion of phenylacetylene was observed on increasing the catalyst amount from 1 wt% to 4 wt% over a period of 24 h. After 24 h, an almost steady state was observed for 4 wt% catalyst, whereas with other catalysts amounts (1 wt% and 2 wt%) a further rise in conversion was noticed (Figure 6b).

(iii) The molar ratio of phenylacetylene to aniline was altered from 1:1 to 1:3 while keeping the temperature (110 °C) and the amount of catalyst (2 wt% w.r.t. phenylacetylene) constant. On increasing the amount of aniline, it was noticed that after 48 h the conversion of phenylacetylene for the ratios of 1:3 and 1:1 remained almost the same. A linear increase in the rate of conversion over a period of 24 h was observed for the entire ratio range (Figure 6c).

(iv) The amount of solvent (toluene) was also varied from 0 mL to 6 mL while keeping the temperature (110 °C), catalyst amount (2 wt% w.r.t. phenylacetylene, 0.1×10^{-2} mmol of Au), and ratio of phenylacetylene and aniline (1:2) constant. It was found that on increasing the solvent amount (6 mL) conversion decreases owing to the decrease in the concentration of phenylacetylene (Figure 6d).

(v) The effect of solvent on the rate of conversion of phenylacetylene was also studied by keeping the temperature (110 °C), catalyst amount (2 wt% w.r.t. phenylacetylene, 0.1×10^{-2} mmol of Au), and ratio of phenylacetylene and aniline (1:2) constant. It was found that the conversion was lower in polar solvents and in the absence of solvents the conversion reached a maximum (Table 2). Polar solvents retard the reaction rate owing to the strong adsorption between solvent and support, which hinders the availability of the reactant.

(vi) The effect of pressure was also studied on the rate of conversion of phenylacetylene and it was found that on applying a pressure of 10 bar, conversion increases; however, the selectivity of the product decreases, which leads to the formation of coupling between phenylacetylene units.

To investigate further the scope and limitations of our catalyst GNP@MCN, the reactions of different alkynes with different aniline derivatives (Table 3) were examined. Aromatic alkynes were more reactive than aliphatic alkynes. The nature of the substituents on both alkynes and anilines had a significant effect on hydroamination. Alkynes and anilines with electron-donating substituents ($-CH_3$) provided better yields whereas analogs with electron-withdrawing substituents ($-Cl$, $-NO_2$) possessed less reactivity. Owing to the strong electron-withdrawing effect of the $-NO_2$ group, no reaction was observed for 4-nitroaniline. The lower yield in the case of both the reactants possessing electron-donating substituents with respect to the reactants itself (entries 2, 3, and 5) might be a result of the steric hindrance between the substituted reactants and the gold supported on the nitrogen-rich mesoporous carbon. In all cases, selectivity for the Markovnikov product was observed.

Different weight percentages of gold were loaded onto the supporting MCN and the variation in conversion is given in Table 4. It was noticed that with an initial increase in the amount of gold, conversion increases; however, on further increasing the amount, the conversion decreases owing to the agglomeration of gold nanoparticles on the surface of the sup-

Table 2. Effect of solvent variation on the hydroamination reaction of phenylacetylene with aniline by using GNP@MCN as the catalyst.[a]

Entry	Solvent	Conversion [mol%]	Selectivity [%]	Yield [mol%]
1	No solvent	87	98	85
2	Toluene	66	98	65
3	Benzene	52	99	51
4	Acetonitrile	1	100	1

[a] Conditions: amine/alkyne = 2:1, 2 wt% catalyst (w.r.t. phenylacetylene, 0.1×10^{-2} mmol of Au), temperature = 110 °C, time = 48 h. Yields were determined by GC and GC-MS analysis. Selectivity for the Markovnikov product was observed in each case.

Table 3. Hydroamination of different alkynes with amines by using GNP@MCN.[a]

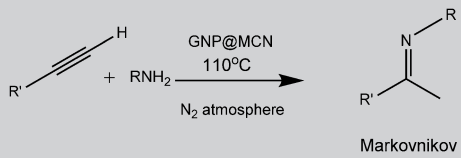

Markovnikov

Entry	R^I	R	Selectivity [%]	Yield [mol%]
1[b]	C_4H_9	C_6H_5	99	20
2	C_6H_5	C_6H_5	98	75
3	4-$CH_3C_6H_4$	C_6H_5	98	52
4[c]	1-ClC_6H_4	C_6H_5	99	29
5	C_6H_5	4-$CH_3C_6H_4$	99	56
6	C_6H_5	2-ClC_6H_4	99	45
7[c]	C_6H_5	4-$O_2NC_6H_4$	–	NR

[a] Conditions: amine/alkyne = 2:1, 2 wt% catalyst (w.r.t. alkyne, 0.1×10^{-2} mmol of Au), temperature = 110 °C, time = 24 h, without solvent. Yields were determined by GC and GC-MS analysis. Selectivity for the Markovnikov product was observed in each case. [b] Reaction temperature = 75 °C. [c] Reaction was performed in 3 mL toluene.

Table 4. Hydroamination of phenylacetylene with aniline by using different wt% of gold loading on the support (Th = Theoretical and Exp = Experimental from ICP-AES.)[a]

Entry	Gold loading [wt%]		Conversion [mol%]	Particle size of Au in GNP@MCN [nm]	TON
	Th	Exp			
1	1	0.7	67	5	93×10^6
2	2	1.8	77	5–10	42×10^6
3	4	3.6	71	15–25	19×10^6

[a] Conditions: amine/alkyne = 2:1, 2 wt% catalyst (w.r.t. phenylacetylene), temperature = 110 °C, time = 24 h, without solvent. Yields were determined by GC and GC-MS analysis. Selectivity for the Markovnikov product was observed in each case. TON = turnover number; TON = moles of desired product formed/number of moles of active sites.

port. Thus, an increase in gold loading results in an increase in the particle size (Figure S2, in the Supporting Information), which affects the activity of the catalyst. It has been found that the catalyst possessing a particle size of around 5 nm is highly active towards hydroamination, whereas an increase in particle size results in lower activity for the same. The vital role of the nitrogen functionalities within the nitrogen-rich mesoporous carbon (MCN) has also been explained through the MCN acting as a size-controlling and stabilizing agent for the controlled growth of gold nanoparticles. A similar control experiment with phenylacetylene and aniline over gold nanoparticles embedded on mesoporous carbon (MC) has also been performed and the conversion was found to be 28% after 24 h, which reveals that despite the formation of gold nanoparticles on the surface of the support, the absence of nitrogen functionalities led to uncontrolled growth and agglomeration of the particles. Separate experiments were performed in the absence of a catalyst and with Au-free MCN. The reaction did not proceed without catalyst and yields were very low (around 2%) with Au-free MCN.

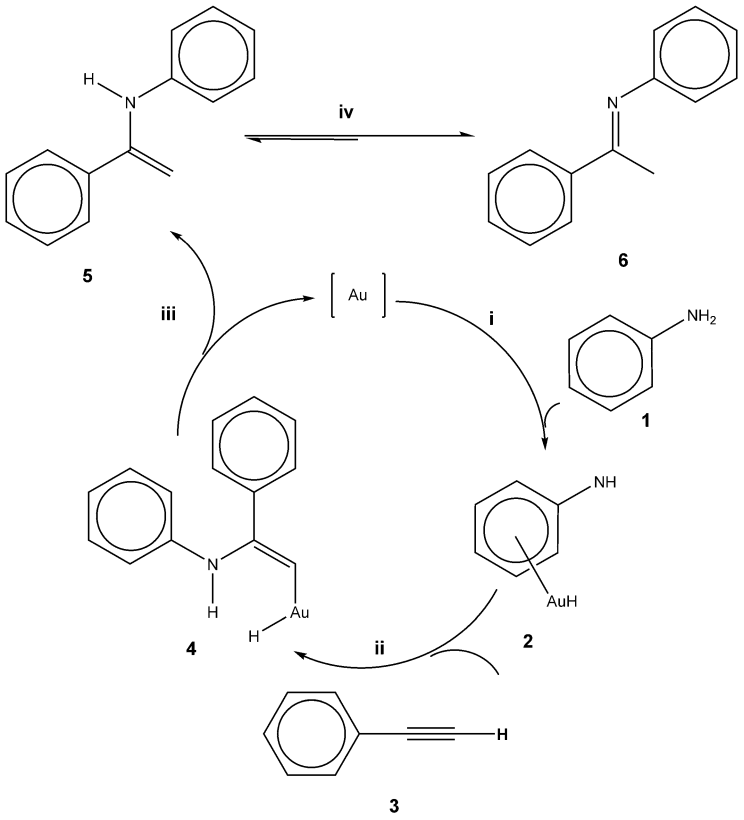

Scheme 3. A plausible mechanism for hydroamination of an alkyne with an amine by using GNP@MCN as a heterogeneous catalyst.

2.3. Mechanistic study

In principle, there are several mechanisms for N–H bond addition to C–C multiple bonds and the catalyst plays a vital role for selectivity and efficacy, however, catalysis in hydroamination can be divided roughly into four sorts: (a) C–C multiple bond activation through the formation of a π-coordinated Lewis acidic metal complex followed by nucleophilic addition by the N-nucleophile moiety; (b) activation of amine to generate a metal–amide complex monitored by insertion of olefin; (c) initial formation of a metal–hydride followed by migratory insertion of olefin into the M–H bond; and (d) rearrangement of initially formed metal–alkyne complex followed by nucleophilic attack by the nucleophile.[12]

Several studies have reported the hydroamination of alkynes, allenes, and alkenes by using Au^{+1} complexes, which follow the route of C–C multiple bond activation by π-coordination followed by addition of the nucleophile;[21] however, it has not yet been established that the mechanistic pathway is the same for Au^0 complexes used as a heterogeneous catalyst. As part of the continuing interest in the development of hydroamination catalysts, in this article a plausible mechanistic pathway of addition of a N-nucleophile across the C–C multiple bond is presented for the Au^0 catalyst GNP@MCN, which involves: (i) oxidative addition of the N–H bond of amine **1** to Au^0 from the gold nanoparticles supported on MCN, giving the amido–aurium complex **2**; (ii) coordination of the π-electrons of alkyne **3** to the Au center of the amido–aurium complex, which forms an intermediate that rearranges through subsequent nucleophilic attack by the N atom to the second alkyne C atom, giving vinyl aurium species **4**; (iii) reductive elimination of enamine **5** from the vinyl aurium species to reproduce the Au^0 cluster; (iv) finally, enamine **5** tautomerizes to give the Markovnikov product **6** (Scheme 3). To understand and verify the proposed mechanism, density functional theory (DFT)-based calculations were performed by using the Gaussian 09 package.[22] All the minimum energy structures for the reactants, products, and intermediates were confirmed as the harmonic vibrational frequency without any imaginary mode. Transition states were confirmed as having one imaginary mode of vibration along the suspected bond breaking or bond making direction. Activation energies were calculated from the free energy differences between the transition states and reactants. The convergence thresholds were set to 0.000015 Hartree/Bohr for the forces, 0.00006 Å for the displacement, and 106 Hartree for the energy change. All calculations were performed with DFT with the unrestricted Beck's three-parameter hybrid exchange functional[23] combined with the exchange component of Perdew and Wang's 1991 functional,[24] abbreviated as B3PW91. The Lanl2dz basis set has been used for all calculations, which is available in the Gaussian 09 package and this basis set has been used because for gold (Au), only this series of basic functions are available.

The stabilization of the GNP catalyst over the MCN support has been studied. As the particle size is nearly 5 nm, for the theoretical study a tetranuclear gold cluster (Au_4) on the MCN support (Figure 7) has been used. The absorption energy of

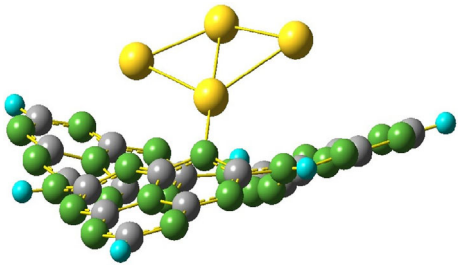

Figure 7. Tetranuclear gold cluster on the MCN support.

Au_4 on the MCN surface is -14.32 kcal mol^{-1}. Thus, there is no need for an extra stabilizing agent for GNP stabilization.

The first step of the reaction pathway considering the aniline activation leads to the formation of intermediate-1 (Figure 8), which involves Au–H and Au–N bond formation via the formation of transition state-1 (Figure S3, in the Supporting Information).

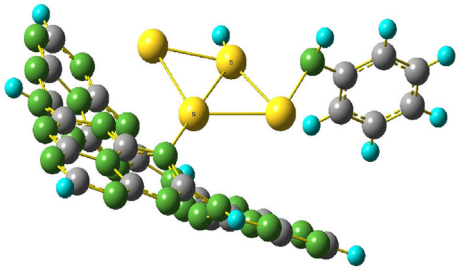

Figure 8. Intermediate-1.

This is similar to that hypothesized in alcohol oxidation by gold catalysts, in which the reaction occurs on two adjacent gold atoms of the nanoparticle surface.[25] In intermediate-1, it is observed that the nitrogen atom attaches to one Au atom and the hydrogen atom bonds to the adjacent Au atom. From natural bond orbital (NBO) analysis[26] of this complex, it was found that lone pair (LP) of the nitrogen atom is donated to BD* of the Au atom. The activation energy for this step is 46.35 kcal mol^{-1}.

Intermediate-1 reacts with the alkyne to form intermediate-2 (Figure 9) via transition state-2 (Figure S4, in the Supporting Information). This involves coordination of the π-electrons of the C≡C bond of alkyne to the Au atom that is attached to the nitrogen atom. As a result of this electron co-ordination, the (N)Au–Au(H) bond opens up and a new Au–N bond is formed. The activation energy of this process is 58.39 kcal mol^{-1}.

On reduction, intermediate-2 rearranges to form Au^0 and the enamine (Figure 10a). This rearrangement passes through transition state-3 (Figure S5, in the Supporting Information), which requires an activation energy of 87.20 kcal mol^{-1}. The total process is presented in an energy profile diagram (Figure 11). The enamine finally tautomerizes to give the targeted imine (Figure 10b). Calculation of the activation energy for this process without catalyst has also been performed and was found to be 159.81 kcal mol^{-1}. The difference in the activation energies with and without catalyst shows the importance of the catalyst GNP@MCN.

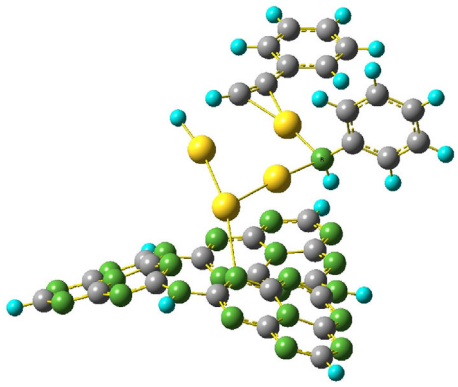

Figure 9. Intermediate-2.

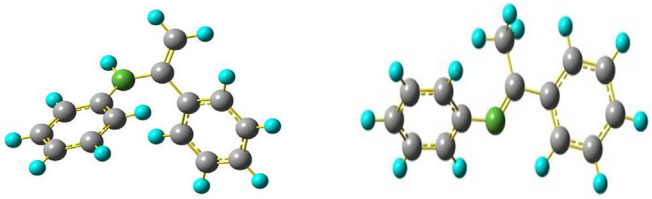

Figure 10. (a) Target enamine and (b) target imine.

2.5. Catalyst recyclability and stability

To study the recyclability and stability of the catalyst GNP@MCN, the reaction was performed at 110 °C with 25 mg (2 wt% w.r.t. phenylacetylene) catalyst and using a phenylacetylene to aniline molar ratio of 1:2 (Table 5).

The fresh catalyst gave 77% conversion of phenylacetylene. For the recyclability test, the catalyst was separated by centrifuging the reaction mixture after the first run, it was then washed several times with acetone and dried at 100 °C under vacuum for 5 h. The catalyst was used with a fresh reaction mixture in the second run and the procedure was repeated for four runs. The results show that the conversion of phenylacetylene was nearly the same in all four runs with ultimately con-

Table 5. Recyclability tests of GNP@MCN in the hydroamination of phenylacetylene with aniline, showing selectivity for the desired product, turnover numbers (TONs) of the catalyst, and wt% of gold loaded on support (ICP-AES).

Run	Gold loading [wt%]	Selectivity [%]	TON
1	1.8	99	42×10^6
2	1.8	99	40×10^6
3	1.8	99	38×10^6
4	1.8	99	37×10^6

Reaction conditions: phenylacetylene/aniline (1:2 molar ratio), catalyst 2 wt% (w.r.t. phenylacetylene), temperature = 110 °C. TON = moles of desired product formed/number of moles of active sites.

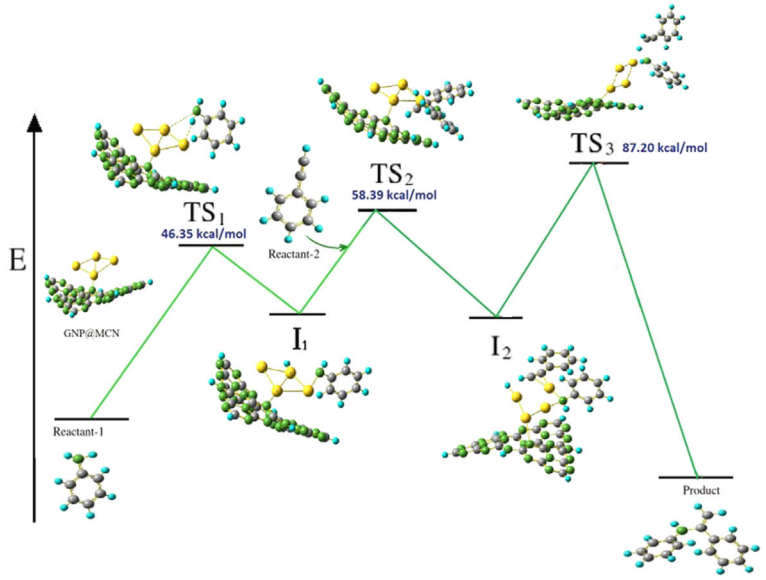

Figure 11. Energy profile diagram for different intermediates and transition states in the hydroamination of phenylacetylene with aniline by using GNP@MCN as the catalyst.

stant selectivity (99%; Figure 12), suggesting that GNP@MCN can be used in repeated cycles without any loss in activity. A nominal decrease in conversion occurred after each cycle, which mainly resulted from handling losses and was not a result of leaching of the active catalyst into the reaction medium. The catalyst stability was also verified by performing a leaching test, in which GNP@MCN was heated at reflux with phenylacetylene and aniline (1:2 molar ratio) at 110 °C for 12 h, then the mixture was cooled and the catalyst was separated by filtration. The filtrate (reaction mixture) was again heated at reflux at 110 °C for another 12 h, which gave no additional conversion and ascertained the absence of metal leaching. The mother liquor was also analyzed by using inductively coupled plasma atomic emission spectroscopy (ICP-AES) to check for metal leaching. Thus, the catalytic activity of studied catalyst system is found to be truly heterogeneous and at the same time the probability of catalyst deactivation is also very low.

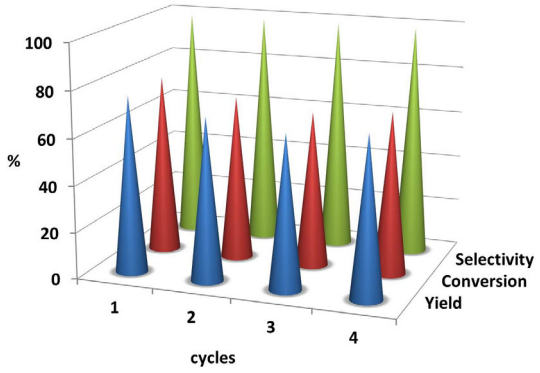

Figure 12. Recyclability test of GNP@MCN for hydroamination of phenylacetylene with aniline showing the conversion of phenylacetylene, corresponding selectivity, and yield of desired product. Reaction conditions: phenyl acetylene/aniline (1:2 molar ratio), catalyst 2 wt% (w.r.t. phenylacetylene), temperature = 110 °C.

Conclusions

Gold nanoparticles (GNPs) have been synthesized and stabilized by an in situ process and incorporated on nitrogen-rich mesoporous carbon (MCN). The catalyst system exhibits very good catalytic activity and above 98% selectivity towards the Markovnikov addition product in the hydroamination of phenylacetylene with aniline with high turnover numbers. The nitrogen functionalities of MCN play a significant role in the controlled growth of the GNPs and stabilization of the zero oxidation state of gold. The optimum reaction conditions were evaluated by varying the temperature, solvent, molar ratio of reactants, and the catalyst concentration. It was observed that conversion of phenylacetylene increases on increasing the temperature and catalyst concentration. The best yield was achieved in the solvent-free system. Characterization techniques such as SEM and TEM show that particles are present in two different environments; some particles are within the mesochannels whereas others are on the surface of the MCN. To predict the mechanistic pathway, a DFT study has been performed by using a tetranuclear gold cluster (Au_4), which ties in with the size of the GNPs (5–6 nm) stabilized on the MCN support. Recyclability tests up to four cycles have been performed, which show a low probability for deactivation and leaching. Hence, GNP@MCN has been found to be a stable, very efficient, and truly heterogeneous catalyst system for selective hydroamination.

Experimental Section

General considerations

All reactions were performed under an inert atmosphere of nitrogen by using Schlenk techniques. Ethylenediamine, carbon tetrachloride, sodium hydroxide, chloroauric acid (99.999%), sodium cit-

rate (>99%), sodium borohydride (98%), phenylacetylene, aniline, anhydrous toluene, benzene, and acetonitrile (HPLC grade) were purchased from Sigma–Aldrich. All the chemicals and solvents were used without further purification.

The X-ray diffraction (XRD) patterns of GNP@MCN were collected with a Bruker D8 advance X-ray diffractometer fitted with a Lynx eye high-speed strip detector and a CuK_α radiation source using CuK_α radiation with a wavelength of 1.5418 Å. Diffraction patterns in the 0.5°–85° region were recorded at a rate of 0.5 degrees (2θ) per minute. The resulting XRD profiles were analyzed to check the structure of MCN before and after incorporation of gold nanoparticles. SEM images of GNP@MCN were taken with an FEI Quanta 200F, using a tungsten filament doped with lanthanum hexaboride (LaB_6) as an X-ray source, fitted with an ETD detector with high vacuum mode using secondary electrons and an acceleration tension of 10 or 30 kV. Samples were analyzed by spreading them on carbon tape. TEM images were recorded with a JEM 2100 (JEOL, Japan) microscope, and samples were prepared by mounting an ethanol-dispersed sample on a lacey carbon formvar coated Cu grid. Elemental mapping was collected with the same spectrophotometer. X-ray photoelectron spectroscopy (XPS) was performed with a Thermo Scientific K-Alpha XPS instrument and binding energies (±0.1 eV) were determined with respect to the C1s peak at 284.8 eV. The porous properties of MCN before and after incorporation of GNPs were examined by nitrogen adsorption–desorption isotherms at 180 °C (Belsorbmax, BEL, Japan) using the Brunauer–Emmett–Teller (BET) equation. Pore size distributions were determined by using the Barrett–Joyner–Halenda (BJH) cylindrical pore approximation. The percentage of gold loading in MCN was confirmed by inductively coupled plasma atomic emission spectroscopy (ICP-AES) by using a PS 3000 UV (DRE), Leeman Labs Inc. (USA). Fourier transform infrared (FTIR) spectra were recorded with a Thermo Nicolet 8700 (USA) instrument with the following operating conditions: resolution = 4 cm^{-1}, scans = 36, operating temperature = 23–25 °C, and frequency range = 4000–500 cm^{-1}. Spectra in the lattice vibrations range were recorded for wafers of sample mixed with KBr.

Synthesis of nitrogen-rich mesoporous carbon (MCN)

In a typical synthesis, calcined SBA-15 synthesized as reported by Zhao et al.[27] was added to a mixture of ethylenediamine and carbon tetrachloride. The mixture was heated at reflux at 90 °C with stirring for 6 h. The acquired dark-brown solid was dried in an oven at 100 °C for 12 h and then ground into a fine powder followed by heat treatment in a nitrogen flow of 50 mL per minute at 600 °C for 5 h with a heating rate of 0.5 °C per minute and kept under 600 °C for carbonization of the polymer. Finally, the MCN was recovered after removal of the silica framework by heating at reflux in 2 M sodium hydroxide solution followed by filtration, several washings with ethanol, and drying at 100 °C.

Synthesis of GNP@MCN

Chloroauric acid ($H[AuCl]_4$) was used as a metallic salt precursor for the synthesis of gold nanoparticles (GNPs). Here, the decoration of GNP@MCN was performed by in situ reduction of $H[AuCl]_4$ with sodium citrate and sodium borohydride. Typically, MCN was dispersed in an aqueous solution of sodium citrate (5.4 mM) followed by ultrasound sonication for 2.5 h. Here, sodium citrate acts not only as a reducing agent but also at the same time maintains the pH of the solution, acts as a surfactant, and enables the efficient dispersion of MCN. The obtained mixture was then transferred to a boiling flask followed by addition of $H[AuCl]_4$ (2 mL, 2 mM) and a freshly prepared aqueous solution of sodium borohydride (112 mM, 100 μL). Sodium borohydride is a strong reducing agent, which enhanced the full reduction of $H[AuCl]_4$. The mixture was then heated at reflux at 100 °C for 12 h, cooled to room temperature, centrifuged, and washed several times with an acetone/water (1:1) mixture. Finally, the obtained GNP@MCN was dried under vacuum at 70 °C for 1 h and stored in a dark and cool place. The gold content in the supporting MCN was verified by ICP-AES analysis and is around 2 wt% (0.4×10^{-2} mmol of Au).

Catalysis with GNP@MCN (hydroamination)

Typically, GNP@MCN (10 mg, 2 wt% w.r.t. phenyl acetylene, 0.1×10^{-2} mmol of Au) was added to a mixture of phenylacetylene and aniline (1:2 molar ratio). The resulting mixture was bath-sonicated for 5 mins for efficient dispersion of the catalyst and then heated at reflux at 110 °C with stirring under an N_2 atmosphere over a period of 24 h. At the end of the reaction, the catalyst was separated by filtration and the product was analyzed by gas chromatograph (GC, Agilent 7890) with an HP5 capillary column (30 m length, 0.28 mm id, 0.5 μm film thickness) and flame ionization detector (FID). Phenylacetylene conversion and the selectivity of the product were calculated by using calibration curves (obtained by manual injection of authentic standard compounds). The product identification was performed by injecting authentic standard samples in GC and GC-MS. To study the effect of pressure, the reaction was performed in a 50 mL stainless steel bomb with nitrogen gas applying a pressure of 10 bar.

Acknowledgments

A.B. gratefully acknowledges CSIR, India for funding CSC-0125, the Director, CSIR-IIP for his help and encouragement. S.D. thanks UGC for a fellowship. The authors also thank the analytical science division, Indian Institute of Petroleum, for analytical services.

Keywords: density functional calculations · gold · hydroamination · mesoporous carbon · nanoparticles

[1] D. A. Giljohann, D. S. Seferos, W. L. Daniel, M. D. Massich, P. C. Patel, C. A. Mirkin, *Angew. Chem. Int. Ed.* **2010**, *49*, 3280–3294; *Angew. Chem.* **2010**, *122*, 3352–3366.
[2] H. Schmidbaur, *Naturwiss. Rundsch.* **1995**, *48*, 443–451.
[3] G. C. Bond, P. A. Sermon, G. Webb, D. A. Buchanan, P. B. Wells, *Chem. Commun.* **1973**, 444b–445.
[4] T. Kobayashi, M. Haruta, H. Sano, M. Nakane, *Sens. Actuators* **1988**, *13*, 339–349.
[5] G. J. Hutchings, *J. Catal.* **1985**, *96*, 292–295.
[6] a) G. Dyker, *Angew. Chem. Int. Ed.* **2000**, *39*, 4237–4239; *Angew. Chem.* **2000**, *112*, 4407–4409; b) A. S. K. Hashmi, T. M. Frost, J. Bats, *J. Am. Chem. Soc.* **2000**, *122*, 11553–11554.
[7] S. Carrettin, M. C. Blanco, A. Corma, A. S. K. Hashmi, *Adv. Synth. Catal.* **2006**, *348*, 1283–1288.
[8] A. Corma, H. Garcia, *Chem. Soc. Rev.* **2008**, *37*, 2096–2126.
[9] a) R. Grisel, K.-J. Weststrate, A. Gluhoi, B. E. Nieuwenhuys, *Gold Bull.* **2002**, *35*, 39–45; b) M. Haruta, *Catal. Today* **1997**, *36*, 153–166; c) A. S. K. Hashmi, G. J. Hutchings, *Angew. Chem. Int. Ed.* **2006**, *45*, 7896–7936; *Angew. Chem.* **2006**, *118*, 8064–8105; d) M. Haruta, *Chem. Rec.* **2003**, *3*, 75–87; e) H. Huang, Y. Zhou, H. Liu, *Beilstein J. Org. Chem.* **2011**, *7*, 897–936.

[10] R. Taube in *Applied Homogeneous Catalysis with Organometallic Compounds: A Comprehensive Handbook in Two Volumes* (Eds.: B. Cornils, W. A. Herrmann), **1996**, Wiley-VCH, Weinheim, pp. 507 – 520.
[11] a) T. E. Müller, M. Beller, *Chem. Rev.* **1998**, *98*, 675 – 704; b) N. Hermanns, S. Dahmen, C. Bolm, S. Bräse, *Angew. Chem. Int. Ed.* **2002**, *41*, 3692 – 3694; *Angew. Chem.* **2002**, *114*, 3844 – 3846.
[12] L. Huang, M. Arndt, K. T. Gooßen, H. Heydt, L. J. Gooßen, *Chem. Rev.* **2015**, *115*, 2596 – 2697.
[13] a) N. Lingaiah, N. Seshu Babu, K. Mohan Reddy, P. S. Sai Prasad, I. Suryanarayana, *Chem. Commun.* **2007**, 278 – 279; b) N. Seshu Babu, K. M. Reddy, P. S. Prasad, I. Suryanarayana, N. Lingaiah, *Tetrahedron Lett.* **2007**, *48*, 7642 – 7645.
[14] V. A. Solovyeva, K. B. Vu, Z. Merican, R. Sougrat, V. O. Rodionov, *ACS Comb. Sci.* **2014**, *16*, 513 – 517.
[15] J. Zhao, Z. Zheng, S. Bottle, A. Chou, S. Sarina, H. Zhu, *Chem. Commun.* **2013**, *49*, 2676 – 2678.
[16] K. Datta, B. Reddy, K. Ariga, A. Vinu, *Angew. Chem. Int. Ed.* **2010**, *49*, 5961 – 5965; *Angew. Chem.* **2010**, *122*, 6097 – 6101.
[17] T. C. Nagaiah, A. Bordoloi, M. D. Sánchez, M. Muhler, W. Schuhmann, *ChemSusChem* **2012**, *5*, 637 – 641.
[18] K. Bomben, J. Moulder, P. E. Sobol, W. Stickle, *Handbook of X-ray Photoelectron Spectroscopy. A Reference Book of Standard Spectra for Identification and Interpretation of XPS data*, Physical Electronics, Eden Prairie, Minnesota, **1995**.
[19] a) S. Kundu, W. Xia, W. Busser, M. Becker, D. A. Schmidt, M. Havenith, M. Muhler, *Phys. Chem. Chem. Phys.* **2010**, *12*, 4351 – 4359; b) R. Arrigo, M. Hävecker, R. Schlögl, D. S. Su, *Chem. Commun.* **2008**, 4891 – 4893; c) V. N. Khabashesku, J. L. Zimmerman, J. L. Margrave, *Chem. Mater.* **2000**, *12*, 3264 – 3270.
[20] J. Xu, L. Zhang, R. Shi, Y. Zhu, *J. Mater. Chem. A* **2013**, *1*, 14766 – 14772.
[21] A. S. K. Hashmi, *Angew. Chem. Int. Ed.* **2010**, *49*, 5232 – 5241; *Angew. Chem.* **2010**, *122*, 5360 – 5369.
[22] Gaussian 09, Revision A. 02, M. J. Frisch, G. W. Trucks, H. B. Schlegel, G. E. Scuseria, M. A. Robb, J. R. Cheeseman, G. Scalmani, V. Barone, B. Mennucci, G. A. Petersson, H. Nakatsuji, M. Caricato, X. Li, H. P. Hratchian, A. F. Izmaylov, J. Bloino, G. Zheng, J. L. Sonnenberg, M. Hada, M. Ehara, K. Toyota, R. Fukuda, J. Hasegawa, M. Ishida, T. Nakajima, Y. Honda, O. Kitao, H. Nakai, T. Vreven, J. A. Montgomery, Jr., J. E. Peralta, F. Ogliaro, M. Bearpark, J. J. Heyd, E. Brothers, K. N. Kudin, V. N. Staroverov, R. Kobayashi, J. Normand, K. Raghavachari, A. Rendell, J. C. Burant, S. S. Iyengar, J. Tomasi, M. Cossi, N. Rega, J. M. Millam, M. Klene, J. E. Knox, J. B. Cross, V. Bakken, C. Adamo, J. Jaramillo, R. Gomperts, R. E. Stratmann, O. Yazyev, A. J. Austin, R. Cammi, C. Pomelli, J. W. Ochterski, R. L. Martin, K. Morokuma, V. G. Zakrzewski, G. A. Voth, P. Salvador, J. J. Dannenberg, S. Dapprich, A. D. Daniels, Ö. Farkas, J. B. Foresman, J. V. Ortiz, J. Cioslowski, D. J. Fox, Gaussian, Inc. Wallingford CT, **2009**.
[23] A. D. Becke, *Phys. Rev. A* **1988**, *38*, 3098.
[24] a) J. P. Perdew, P. Ziesche, H. Eschrig, *Electronic Structure of Solids 91, Vol. 11*, Akademie Verlag, Berlin, **1991**; b) J. P. Perdew, J. Chevary, S. Vosko, K. A. Jackson, M. R. Pederson, D. Singh, C. Fiolhais, *Phys. Rev. B* **1992**, *46*, 6671; c) J. P. Perdew, J. Chevary, S. Vosko, K. A. Jackson, M. R. Pederson, D. Singh, C. Fiolhais, *Phys. Rev. B* **1993**, *48*, 4978; d) J. P. Perdew, K. Burke, Y. Wang, *Phys. Rev. B* **1996**, *54*, 16533.
[25] B. N. Zope, D. D. Hibbitts, M. Neurock, R. J. Davis, *Science* **2010**, *330*, 74 – 78.
[26] F. Weinhold, C. R. Landis, *Valency and Bonding: A Natural Bond Orbital Donor – Acceptor Perspective*, Cambridge University Press, Cambridge, **2005**.
[27] D. Zhao, J. Feng, Q. Huo, N. Melosh, G. H. Fredrickson, B. F. Chmelka, G. D. Stucky, *Science* **1998**, *279*, 548 – 552.

Received: June 24, 2016
Published online on ■■ ■■, 0000

Au hydroamination catalyst: The in situ synthesis of gold nanoparticles in the surface cavity of mesoporous nitrogen-rich carbon (MCN) allowed them to be utilized efficiently as a catalyst in the hydroamination of phenylacetylene with aniline, with more than 98% selectivity towards the Markovnikov addition product. The mechanistic pathway has been studied with DFT-based calculations, which predict the stabilization of tetranuclear Au clusters over the MCN support.

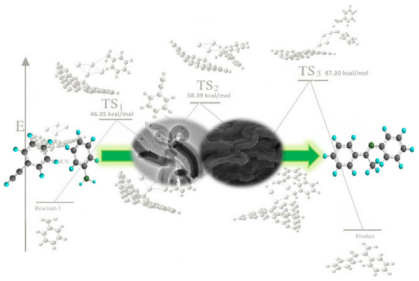

*M. Sengupta, A. Bag, S. Das, A. Shukla, L. N. S. Konathala, C. A. Naidu, A. Bordoloi**

■■ – ■■

Reaction and Mechanistic Studies of Heterogeneous Hydroamination over Support-Stabilized Gold Nanoparticles